Journal of Energy Storage 47 (2022) 103606

Contents lists available at ScienceDirect

Journal of Energy Storage

journal homepage: www.elsevier.com/locate/est

Research Papers

Simulation of mixed-convection of water and nano-encapsulated phase change material inside a square cavity with a rotating hot cylinder

Arsalan Nasiri Sadr [a], Masih Shekaramiz [b], Meysam Zarinfar [c], Amin Esmaily [d], Hamidreza Khoshtarash [e], Davood Toghraie [f,*]

[a] Department of Mechanical and Energy Engineering, Shahid Beheshti University (SBU), Tehran, Iran
[b] Department of Mechanical Engineering, University of Kashan, Kashan, Iran
[c] Department of Civil Engineering, University of Bu-Ali Sina, Hamedan, Iran
[d] Department of Energy, Islamic Azad University, Najafabad Branch, Iran
[e] Department of Mechanical Engineering, Iran University of Science and Technology, Tehran, Iran
[f] Department of Mechanical Engineering, Khomeinishahr Branch, Islamic Azad University, Khomeinishahr, Iran

ARTICLE INFO

Keywords:
Nano-encapsulated PCM
Mixed convection
Rotating cylinder
Square cavity
Melting zone
The ratio of heat capacity

ABSTRACT

Nano-encapsulated PCM consists of a solid shell and a phase change material (PCM) in the core that improves the thermal properties of base fluids. The heat capacity of the nanofluid increases due to the latent heat of the NEPCM core and the heat transfer rate increases dramatically. Also, a phase change occurs in a certain range of temperature. In the present study, the core and shell of NEPCM are n-nonadecane and polyurethane, respectively. Mixed convection of water-NEPCM is simulated inside a square chamber with cold walls and a hot rotating cylinder in the center. Coupled PDE equations are solved by the SIMPLE algorithm and developing C++ code. The parameters of Grashof number, Reynolds number, intensity of stored energy in the core of NEPCM (χ), and fusion temperature (θ_f) have been studied on the flow pattern, temperature contour, heat capacity ratio (Cr) contour, and Nusselt number. Based on this study it can be concluded that in general the optimal state of θ_f is in moderate values or especially numbers close to 0.5 and at this range of θ_f, χ reduction can enhance Nusselt number more. Also, at high *Gr* number by increasing *Re* number, heat transfer rate reduces. The results also show that adding NEPCM can increase the Nusselt number by more than 13%.

1. Introduction

The phase changes of the materials take place at almost constant temperatures. Therefore, significant heat can be given to materials in the two-phase state without changing their temperature. This energy is stored in them as latent energy and have a high ability to be used in cooling electrical components. Also, the phase change process is often used in heat exchangers. A similar process is performed in evaporators for use in cooling systems.

On the other hand, by increasing renewable energy systems applications, the necessity to develop tools for storing electrical energy (batteries) and thermal energy (storage tank) has become more prominent. In recent decades, the use of phase change materials (PCMs) in the application of thermal energy storage has been considered by researchers in diverse fields [1]. Different materials change phase at different temperatures, so the PCMs are used in a wide range of temperatures. There are three types of PCMs: organic, inorganic, and eutectics [2]. Paraffin is an example of PCMs organic classification that has been widely used due to its benefits such as chemical stability [3]. Disadvantages of paraffin include low thermal conductivity. Using the materials in the two-phase state is not facile in some conditions, like using PCM at force convection heat transfer in a solid-liquid phase. Encapsulating PCM inside a sell suggests overcoming this issue and the problem of low thermal conductivity of paraffin [4,5]. These capsules are made in macro, micro, and nanoscales. Nano-encapsulated PCMs (NEPCMs) are nanoscale capsules that contain PCM. NEPCMs are suspended into the base fluid, such as water. By heating the nanofluid, NEPCMs can store high thermal energy at a specific temperature. NEPCMs have a high potential for use in energy storage systems [6]. NEPCMs have performed better due to their high surface area and mechanical and thermal stability [7]. Seyf et al. [8] simulated the forced convection flow of octadecane NEPCM suspended into polyalphaolefin as a base fluid inside a microtube. They observed that increasing the

* Corresponding author.
E-mail address: davoodtoghraie@iaukhsh.ac.ir (D. Toghraie).

https://doi.org/10.1016/j.est.2021.103606
Received 2 August 2021; Received in revised form 6 October 2021; Accepted 10 November 2021
Available online 21 November 2021

Nomenclatures

C_r	the ratio of heat capacity of mixture to water
C_p	specific heat capacity (J/kgK)
f	fusion function
g	gravitational acceleration (m/s^2)
Gr	Grashof number
h_{sf}	latent heat of core (J/kg)
k	thermal conductivity (W/mK)
L	length of the cavity (m)
l	weight ratio of core to shell
Nu_{Ave}	average Nusselt number
p	pressure (Pa)
Pr	Prandtl number
r	radius of the cylinder
Ri	Richardson number
Re	Reynolds number
T	temperature (K)
T_{Mr}	melting temperature range (K)
T_f	fusion temperature (K)
V	velocity vector (m/s)

Greek symbols

α	thermal diffusivity (m^2/s)
β	thermal expansion coefficient $(1/K)$
δ	thickness of melting zone
θ	non-dimensional temperature
λ	the ratio of heat capacity of NEPCM to water
H	length of the cavity
μ	dynamics viscosity (kg/ms)
υ	kinematic viscosity (m^2/s)
ϑ_s	volume ratio of core to shell
ρ	density (kg/m^3)
ω	angular velocity of inner cylinder (rad/s)
χ	the intensity of stored energy in the core

Subscript

bf	base fluid
c	core of the NEPCM
f	fusion
n	nanoparticle
m	mixture of water-NEPCM
l	liquid phase
s	sell of the NEPCM

melting range of NEPCMs increases Nusselt number and reduces thermal resistance. Sabbah et al. [9] investigated force convection heat transfer of MEPCMs into the microchannel to cool electronic components. Their results showed that the use of PCM compared to pure water requires less pumping power to achieve uniform and low temperatures. Seyf et al. [10] also investigated the forced convection heat transfer of water-NEPCM over a square cylinder at a constant temperature. They reported that increasing the NEPCM volume fraction improves heat transfer and increases wall shear stress. The focus of the above papers was more on forced convection flow. But in view of natural convection heat transfer, Zadeh et al. [11] numerically studied the conjugate natural convection and entropy generation in a square cavity. They showed that adding NEPCMs to the base fluid increased the heat transfer rate by 45%, although it increased the Bejan number. Kant et al. [12] investigated the natural convection heat transfer of a thermal storage tank. The authors evaluated the effect of adding nanoparticles to PCM. They added

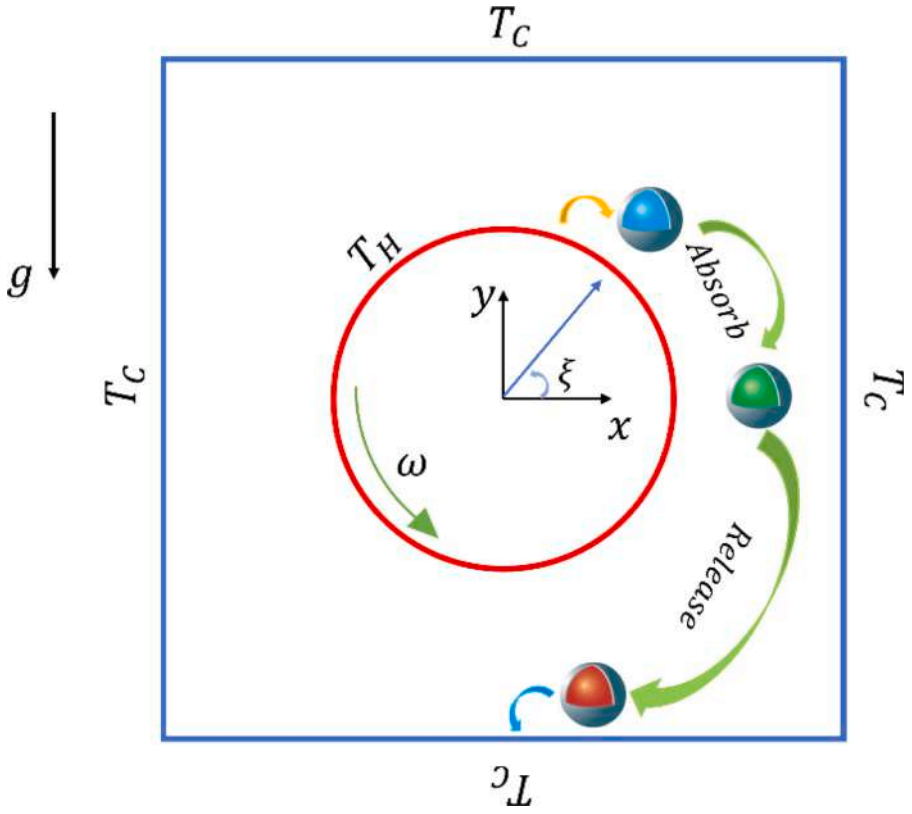

Fig. 1. Schematic of a square chamber and a rotating cylinder in the center and NEPCM particles for present simulation.

different percentages of graphene nanoparticles to three types of PCMs, Capric Acid, CaC_2-$6H_2O$, and n-octadecane. Their results showed that adding graphene to PCMs improves heat transfer. The natural convection of NEPCMs and nanofluids within square [13,14] and cylindrical [15] and semi-annulus [16] cavities has been investigated by several studies. Our focus in this paper is on mixed convection heat transfer. We intend to examine the effect of the two effects of natural and forced convection. Ghalambaz et al. [17] investigated the mixed convection flow of NEPCM on a vertical plate. Their results showed that by reducing the melting temperature of NEPCMs, heat transfer is improved. Raizah et al. [18] simulated numerically the mixed convection heat transfer within a cylindrical geometry with rectangular chambers on either side. They used the ISPH method for the simulation, and one of their results was that as the radius of the rotating cylinder increased, the intensity of the melting zone decreased. Ahmed and Raizah [19] simulated fluid flow and heat transfer due to radiation and convection through a prismatic enclosure. In their study, the core material of NEPCM was nonadecane, and the shell material was polyurethane. The results of the simulation show that the use of NEPCM significantly improves heat transfer. Understanding and studying the evaluation of NEPCMs is restricted compared to the study of the effects of nanoparticles or the configuration of shapes [20–24]. Also, some researchers tried to obtain the properties of different systems that are equipped to nanostructures [25–31]. Few studies have evaluated mixed convection heat transfer in the presence of NEPCMs. In this paper, we try to understand the heat transfer performance of NEPCMs by evaluating and analyzing 135 cases in different Reynolds number, Grashof number, and various properties of NEPCMs. Also, we attempt to establish a significant relationship between heat transfer rate, isothermal lines, streamlines, and heat capacity ratio contours.

2. Problem presentation

The geometry consists of a square chamber with the length $H = 4r$ and a clockwise rotating cylinder with radius r in the center of the chamber (see Fig. 1). Mixed convection of water-NEPCM occurs between the square chamber and the rotating cylinder. The walls of the square chamber are at a constant temperature of T_c and the wall of the rotating cylinder is at a constant temperature of T_h. NEPCM melt with receiving heat from the hot wall and freeze with losing heat in the cold wall.

2.1. Assumptions and equations

Natural and forced convection flow occurs due to the buoyancy force and the rotation of the cylinder, respectively. The combination causes mixed convection. Water and NEPCM flow are two-dimensional, incompressible, and steady-state. The Boussinesq approximation is also considered for linear density changes. The equations of continuity, momentum, and energy in x-y coordinates are as follows [32]:

$$\frac{\partial u}{\partial x}+\frac{\partial v}{\partial y}=0. \tag{1}$$

$$\rho_m\left(u\frac{\partial u}{\partial x}+v\frac{\partial u}{\partial y}\right)=-\frac{\partial P}{\partial x}+\mu_m\left(\frac{\partial^2 u}{\partial x^2}+\frac{\partial^2 u}{\partial y^2}\right). \tag{2}$$

$$\rho_m\left(u\frac{\partial v}{\partial x}+v\frac{\partial v}{\partial y}\right)=-\frac{\partial P}{\partial y}+\mu_m\left(\frac{\partial^2 v}{\partial x^2}+\frac{\partial^2 v}{\partial y^2}\right)+(\rho\beta)_m(T-T_C)g. \tag{3}$$

$$\left(u\frac{\partial}{\partial x}((\rho C_P)_m T)+v\frac{\partial}{\partial y}((\rho C_P)_m T)\right)=k_m\left(\frac{\partial^2 T}{\partial x^2}+\frac{\partial^2 T}{\partial y^2}\right). \tag{4}$$

In the above equations, u and v are the velocity components in the x and y-directions. Also, P, T, and g are pressure, temperature, and gravity acceleration in the y-direction, respectively. Last term in Eq. (3) is buoyant Boussinesq source term. In the energy conservation equation (Eq. (4)), the NEPCMs impacts of advection term. The performance of the NEPCM nanoparticles as well as how they affect the performance of the problem will be described later. To close the above coupled equations, boundary conditions are required. Moreover, the temperature of the square chamber walls is T_c and the temperature of the rotating cylinder is T_h. The boundary conditions of velocity are zero for the cold walls, and tangential velocity at the hot cylindrical wall is $r\omega$. By defining the following dimensionless parameters, we can make dimensionless the governing equations [33,32].

$$(X,\ Y)=\left(\frac{x}{r},\ \frac{y}{r}\right),(U,\ V)=\left(\frac{u}{r\omega},\ \frac{v}{r\omega}\right),\ \theta=\frac{T-T_C}{T_H-T_C},\ p=\frac{P}{\rho_{bf}r^2\omega^2}$$

$$\frac{\partial U}{\partial X}+\frac{\partial V}{\partial Y}=0. \tag{5}$$

$$\left(\frac{\rho_m}{\rho_{bf}}\right)\left(U\frac{\partial U}{\partial X}+V\frac{\partial U}{\partial Y}\right)=-\frac{\partial p}{\partial X}+\frac{1}{Re_{bf}}\left(\frac{\mu_m}{\mu_{bf}}\right)\left(\frac{\partial^2 U}{\partial X^2}+\frac{\partial^2 U}{\partial Y^2}\right). \tag{6}$$

$$\left(\frac{\rho_m}{\rho_{bf}}\right)\left(U\frac{\partial V}{\partial X}+V\frac{\partial V}{\partial Y}\right)=-\frac{\partial p}{\partial Y}+\frac{1}{Re_{bf}}\left(\frac{\mu_m}{\mu_{bf}}\right)\left(\frac{\partial^2 V}{\partial X^2}+\frac{\partial^2 V}{\partial Y^2}\right)+\frac{Gr_{bf}}{{Re_{bf}}^2}\left(\frac{(\rho\beta)_m}{(\rho\beta)_{bf}}\right)\theta. \tag{7}$$

$$\left(U\frac{\partial}{\partial X}(Cr\ \theta)+V\frac{\partial}{\partial Y}(Cr\ \theta)\right)=\frac{1}{Re_{bf}Pr_{bf}}\left(\frac{k_m}{k_{bf}}\right)\left(\frac{\partial^2\theta}{\partial X^2}+\frac{\partial^2\theta}{\partial Y^2}\right). \tag{8}$$

The dimensionless numbers are expressed as follows [32]:

$$\nu_{bf}=\frac{\mu_{bf}}{\rho_{bf}},\ \alpha_{bf}=\frac{k_{bf}}{(\rho c_p)_{bf}},\ Pr=\frac{\nu_{bf}}{\alpha_{bf}},Re_{bf}=\frac{\omega r^2}{\nu_{bf}},and\ Gr_{bf}=\frac{g\beta_{bf}\Delta Tr^3}{{\nu_{bf}}^2}.$$

which ν_{bf}, α_{bf}, Pr, Re_{bf}, *and* Gr_{bf} are kinematic viscosity, thermal diffusion, Prandtl, Reynolds, and Grashof numbers [34]. Also, the dimensionless number appearing in the energy equation is the ratio of the heat capacity of the mixture to the base fluid (Cr) [32].

$$Cr=\frac{(\rho C_P)_m}{(\rho C_P)_{bf}}=1-\varphi+\lambda\varphi+\frac{\varphi}{\chi}f \tag{9}$$

In Eq. (9), subscriptions *m* and *f* are the nanofluid mixture and base fluid, respectively. Specific heat capacity and density of water $(\rho C_P)_{bf}$ are constant. However, for a specific materials of base fluid and NEPCM, the specific heat capacity values of the mixture are a function of the volume fraction of the NEPCMs, the amount of latent heat of the NEPCM core, and temperature (f). φ shows the variability relative to the volume fraction, and χ shows the variability associated with the latent heat of the NEPCM core and λ is calculated by the following equation [33]:

$$\lambda=\frac{\left(C_{p_{c,\ l}}+lC_{p_s}\right)\rho_c\rho_s}{(\rho_s+l\rho_c)(\rho C_P)_{bf}} \tag{10}$$

λ is the ratio of heat capacity of NEPCM in liquid phase to base fluid. Where $c,\ l,$ *and* s are subscripts for core, liquid, and sell respectively. The l coefficient is core-shell weight ratio and equal to 0.447. Also, at Eq. (9) χ is the ratio of an increase in base fluid temperature to energy stored as latent heat in the core [32]:

$$\chi=\frac{C_{P,\ bf}}{h_{sf}/T_{Mr}}\frac{\rho_{bf}(\rho_s+l\rho_c)}{(\rho_s\rho_c)} \tag{11}$$

h_{sf} is latent heat of core and T_{Mr} is melting temperature range of core. Also, the term f in Eq. (9) is the non-dimensional fusion function obtained by the following equation [33]:

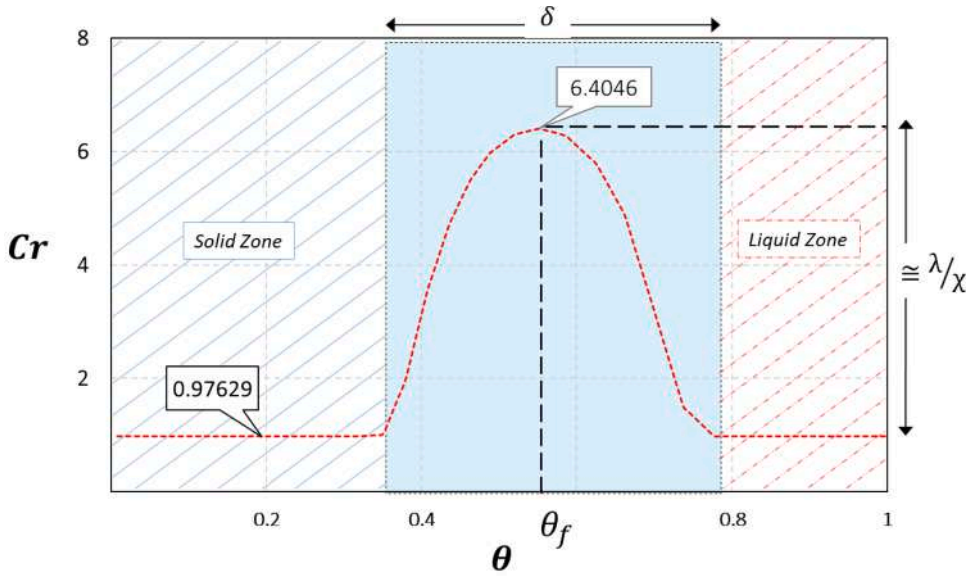

Fig. 2. Schematic of Cr and related parameters in Eqs. (9)–(13).

$$f = \frac{\pi}{2}\sin\left(\frac{\pi}{\delta}\left(\theta - \theta_f + \frac{\delta}{2}\right)\right) \times \begin{cases} 0 \ if \ \theta < \theta_f - \dfrac{\delta}{2} \\ 1 \ if \ \theta_f - \dfrac{\delta}{2} < \theta < \theta_f + \dfrac{\delta}{2} \\ 0 \ if \ \theta < \theta_f + \dfrac{\delta}{2} \end{cases} \tag{12}$$

$$\delta = \frac{T_{Mr}}{\Delta T}, \ and \ \theta_f = \frac{T_f - T_C}{\Delta T} \tag{13}$$

The parameters θ_f, and δ represent the fusion dimensionless temperature, and internal fusion, respectively. In the other word δ is the thickness of the melting zone. By a closer look at Eq. (9) and according to Eq. (12), if the nanofluid temperature is higher than the NEPCM core melting temperature ($T > T_f + \frac{T_{Mr}}{2}$) or lower than the core solidification temperature ($T < T_f - \frac{T_{Mr}}{2}$) the last term of Eq. (9) will be zero, and the values of Cr reduces. Melting temperature values and melting range also affect Cr. By changing the values of Cr heat transfer can be improved. The most important strength of using NEPCMs compared to conventional nanoparticles is the significant increase in specific heat capacity. The coefficient of the function f in Eq. (9) is the amplitude of changing specific heat capacity in the two-phase state. Where, by comparing with Eq. (11), the latent heat of the NEPCM core (h_{sf}) effects on Cr. Fig. 2 graphically represents the effect of the aforementioned parameters on Cr.

Fig. 2 shows that in the part where there is no phase change, the Cr values are less than one because NEPCM has a lower specific heat capacity than water, thus reducing the specific heat capacity of the nanofluid. However, in the part of phase change (highlighted by light blue), the specific heat capacity of the nanofluid increases dramatically. The values of Cr presented for $\chi = 0.01$.

The heat transfer rate can be calculated by the Nusselt number, which is as follows [35–42]:

$$Nu_{loc} = \frac{k_m}{k_{bf}}\frac{\partial\theta}{\partial n}, \quad Nu_{Ave} = \frac{1}{\pi D}\int Nu_{loc}(n)dn. \tag{14}$$

where Nu_{loc} is local Nusselt number and D is diameter of inner cylinder, and Nu_{Ave} is average Nusselt number.

2.2. Thermophysical properties

Nano-encapsulated PCM consist of a polyurethane shell and an n-nonadecane core. The n-nonadecane is a desirable organic phase change material for thermal energy storage, melting and solidifying occur at temperature range of 31°C and melting latent heat of 156.07 kJ/kg and solidifying latent of 164.99 kJ/kg. Therefore, can be utilized in buildings for thermal energy storage, and the operating temperature range and the amount of energy that can be stored make this PCM possible for use in buildings [43]. The polyurethane shell has high elastic properties, strength, smooth surface [44] and low crystallinity [45], so it has been considered by researchers. Also, this shell does not have environmental and health problems related to formaldehyde release. Also, based on previous experimental studies [46], the thermophysical properties of water and the mentioned NEPCM have been extracted. Also, studies on the preparation of these nanoparticles for similar applications were presented [47]. Thermophysical properties of NEPCM can be introduced by considering both thermophysical properties of core and shell as follows [32]:

$$\rho_n = \frac{(1+l)\rho_c\rho_s}{\rho_s + l\rho_c} \tag{14a}$$

where n indicates nanoparticle subscription. The specific heat capacity of the core can be expressed as a Sinusoidal function, whose argument is a function of temperature, fusion temperature (T_f), and phase change temperature range (T_{Mr}) as mentioned before. Also, whose amplitude is a function of latent heat of core (h_{sf}), T_f, and the specific heat capacity of the core in liquid state ($C_{p_{c,\,l}}$). Moreover, specific heat capacity of the NEPCM core ($C_{p,\,c}$) in the phase change temperature range is [33]:

$$C_{p,\,c} = C_{p\,c,l} + \left\{\frac{\pi}{2}\left(\frac{h_{sf}}{T_{Mr}} - C_{p\,c,l}\right)\left(\sin\pi\frac{T - (T_f - T_{Mr}/2)}{T_{Mr}}\right)\right\} \times \begin{cases} 0 \ if \ T < T_f - \dfrac{T_{Mr}}{2} \\ 1 \ if \ T_f - \dfrac{T_{Mr}}{2} < T < T_f + \dfrac{T_{Mr}}{2} \\ 0 \ if \ T < T_f + \dfrac{T_{Mr}}{2} \end{cases} \tag{15}$$

The specific heat capacity and thermal expansion coefficient of NEPCM can be introduced as follows [32]:

Table 1
Thermophysical properties of materials used at 303 K [32,49].

Property / Material	$\rho\left(\frac{kg}{m^3}\right)$	$C_p\left(\frac{J}{kgK}\right)$	$\beta \times 10^{-5}\left(\frac{1}{K}\right)$	$k\left(\frac{W}{mK}\right)$	$\mu \times 10^{-6}\left(\frac{kg}{ms}\right)$
water†	995.6	4180	21	0.615	797
n − nonadecane *	786	1317	50	0.19	–
*polyurethane***	721	2037	17.3	0.025	–

† Base fluid.
* Core.
** Sell.

$$C_{p,\ n} = \frac{(C_{p,\ c} + lC_s)\rho_c\rho_s}{(\rho_s + l\rho_c)\rho_n} \tag{16}$$

$$\beta_n = \beta_c + \left(\frac{\beta_s - \beta_c}{2}\right)\left(1 - \frac{l\rho_s}{\rho_c}\right) \tag{17}$$

The thermophysical properties of the water-NEPCM mixture can be classified as Table 1 by considering the thermophysical properties of water, NEPCM nanoparticles, and NEPCM volume fraction. Thermophysical equations of the mixture including density, specific heat capacity, and thermal expansion coefficient are listed below [32,48].

$$\rho_m = (1-\varphi)\rho_{bf} + \varphi\rho_n \tag{18}$$

$$C_{P,\ m} = \frac{(1-\varphi)\rho_f C_{P,b\ f} + \varphi\rho_n C_{P,\ n}}{\rho_m} \tag{19}$$

$$\beta_{\ m} = \frac{(1-\varphi)\rho_{bf}\beta_{bf} + \varphi\rho_n\beta_n}{\rho_m} \tag{20}$$

In all of the equations, the m, n, c, and s index represent the mixture, NEPCM, core, and shell, respectively. The present simulation has been studied at a constant volume fraction of 0.035. Therefore, according to reference [46], the dynamic viscosity and thermal conductivity of the mixture at 303K are equal to 0.7 $W/m.K$ and 122 $\times$ $10^{-5} kg/m.s$, respectively. The thermophysical properties of the materials are also listed in Table 1.

2.3. The numerical setting, grid independency, and validation

Equations and boundary conditions are solved by developing the C++ code of OpenFOAM software. The FVM method is used with the SIMPLE algorithm to solve the velocity and pressure fields for mixed convection of water-NEPCM. The relaxation factors for velocity, pressure and temperature are 0.2, 0.4, and 0.7, respectively, and the residual of fields is less than 10^{-6}. Also, the grid independency is studied for critical conditions $Gr_{bf} = 10^4, Re_{bf} = 50, \chi = 0.01, \theta_f = 0.5$. Fig. 3 represents the average Nusselt number of grid independency. Observations show that the 28,000 mesh is suitable for simulation. For the present simulation, boundary layer mesh is applied near all walls and triangular mesh is used for between the walls.

Table 2 presents the validation of free convection of $water - Al_2O_3$ nanofluid at different Ra numbers for Pr = 4.62, and $\varphi_{ave} = 0.03$. The results of Nu_{Ave} are compared with numerical and experimental results. Relative error (ε) is calculated as $\left(\varepsilon = \frac{Nu(Present\ study) - Nu(Previous\ Study)}{Nu(Present\ study)} \times 100\right)$. The results are in good agreement. Also, NEPCM part of the present work is validated with numerical results of Ghalambaz et al. [33] for natural convection of water-NEPCM inside a cavity. Fig. 4 shows Cr and temperature counters in the conditions $Ra = 10^5, \delta = 0.05, Ste = 0.313, Pr = 6.2, \theta_f = 0.3$ *and* $\theta_f = 0.5$. The contours of both works are close and validation is good for the current simulation of NEPCM.

The last two validations were for free convection. To validate the mixed-convection, streamlines, isothermal lines, and local and average Nusselt numbers are given in Fig. 5. The results are convincing.

3. Results and discussion

The results presented for different Grashof $(10^2 \le Gr \le 10^4)$ and Reynolds numbers $(0.5 \le Re \le 50)$ at fixed $\delta = 0.2, \varphi = 0.035, Pr = 5.42$ and different χ (0.01, 0.02 and 0.4) and θ_f (0.1–0.9). Streamlines, isothermal lines, Cr contours and Nusselt numbers are shown for evaluation. Fig. 6 illustrates the streamlines. For low Gr numbers, the forced convection flow is predominant in comparison to natural convection, and as Re increases, the forced convection effect intensifies. According

Table 2
Comparison of Nu_{Ave} for free convection of water − Al_2O_3 nanofluid.

	$Ra = 10^6$	$Ra = 1.35 \times 10^6$	$Ra = 1.68 \times 10^6$
*Present Study**	9.3665	10.0636	10.7606
Shiekhzade et al [51]. *	9.1495 ($\varepsilon = 2.3\%$)	9.5617 ($\varepsilon = 5.2\%$)	10.5079 ($\varepsilon = 2.3\%$)
Ho et al [52].**	8.9683 ($\varepsilon = 4.2\%$)	9.3445 ($\varepsilon = 7.1\%$)	9.8282 ($\varepsilon = 8.7\%$)

* Numerical.
** Experimental.

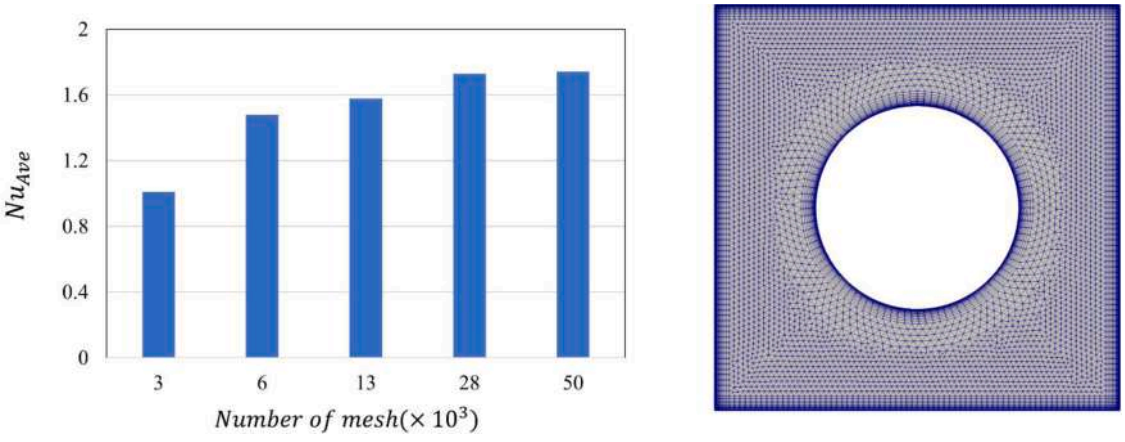

Fig. 3. Schematic of the used mesh and the grid independency plot for the average Nusselt number.

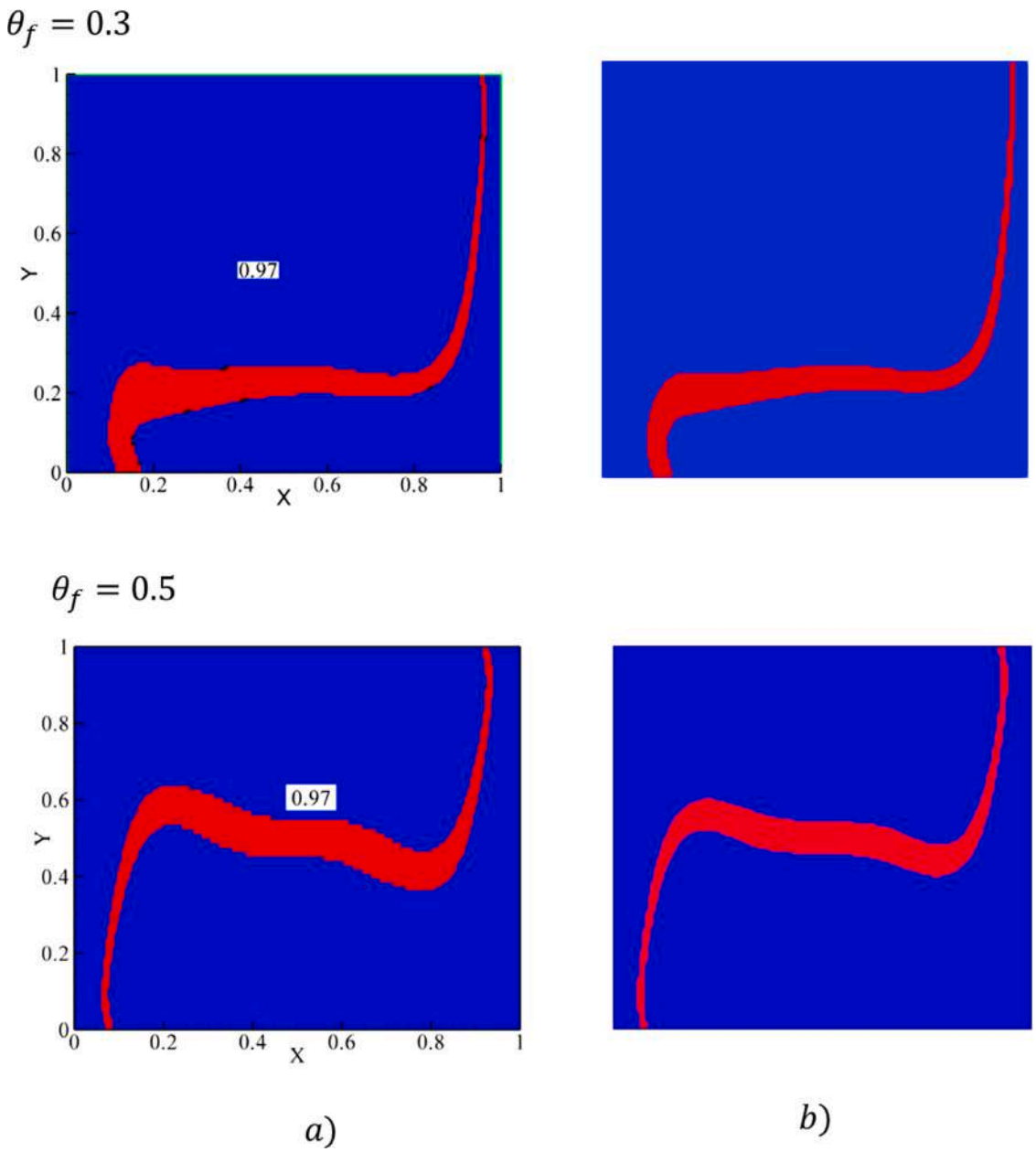

Fig. 4. Heat capacity ratio (Cr) contours for $Ra = 10^5$, $Ste = 0.313$, $Pr = 6.2$, $\theta_f = 0.3$, and $\theta_f = 0.5$ (a) Ghalambaz et al. [33] and (b). Present work.

to the ratio of $\frac{U}{r\omega}$, it is determined that in the lower Gr, the maximum ratio is equal to one. In other words, it shows that the velocity of natural convection is almost negligible.

At higher *Gr* numbers (Gr = 1000) and low *Re* number the maximum ratio of $\frac{U}{r\omega}$ is 1.2, which indicates that the presence of natural convection is remarkable, although forced convection is more prevalent. By looking closely at the streamlines, two vortices are observed, which are formed due to natural convection. In the left part of the cavity, the velocity is higher. Because the inner cylinder rotation (clockwise) and natural convection flow at the right side of the cavity have the same direction. By increasing Re, the maximum value of the $\frac{U}{r\omega}$ ratio equals one and forced convection prevails. In $Gr = 10^4$ and low *Re* numbers, the maximum $\frac{U}{r\omega}$ ratio is 5 and the natural convection is much bolder. Also, flow patterns are in the form of natural convection flow [50]. In this *Gr* number, by increasing the angular velocity of the inner cylinder and increasing the *Re* number, the maximum $\frac{U}{r\omega}$ ratio decreases to unit value (at Re=50). Decreasing the $\frac{U}{r\omega}$ ratio at $Gr = 10^4$ indicates the negative effect of the cylinder rotation on the convection.

Fig. 7 illustrates the constant non-dimensional temperature lines (solid black lines) and the Cr contours. Due to NEPCMs melt or freeze at particular temperatures, the red area in Cr contours indicates that the material inside the nano-capsules is in the two-phase state, and their specific heat capacity increases. The values of θ_f indicate the position of the melting on non-dimensional temperature lines (see Fig. 2). By changing the values of θ_f, the region in which the melting occurs will be different. Therefore, according to Fig. 7, it is observed that for $\theta_f = 0.3$ melting occurs at the constant non-dimensional temperature line of 0.3 and this is also true for other θ_fs. The effect of the location of the melting zone on the heat transfer rate will be further described.

Fig. 6 shows that at the high *Gr* number, increasing *Re* intensifies the resistance to natural convection flow and reduces the flow velocity. The diagram of dimensionless temperature lines with Cr contours is presented in Fig. 8. By increasing velocity of flow, the streamlines have changed from distortion to the shape of concentric circles and reduces the concentration of isothermal lines in near the cylinder wall. Also, the

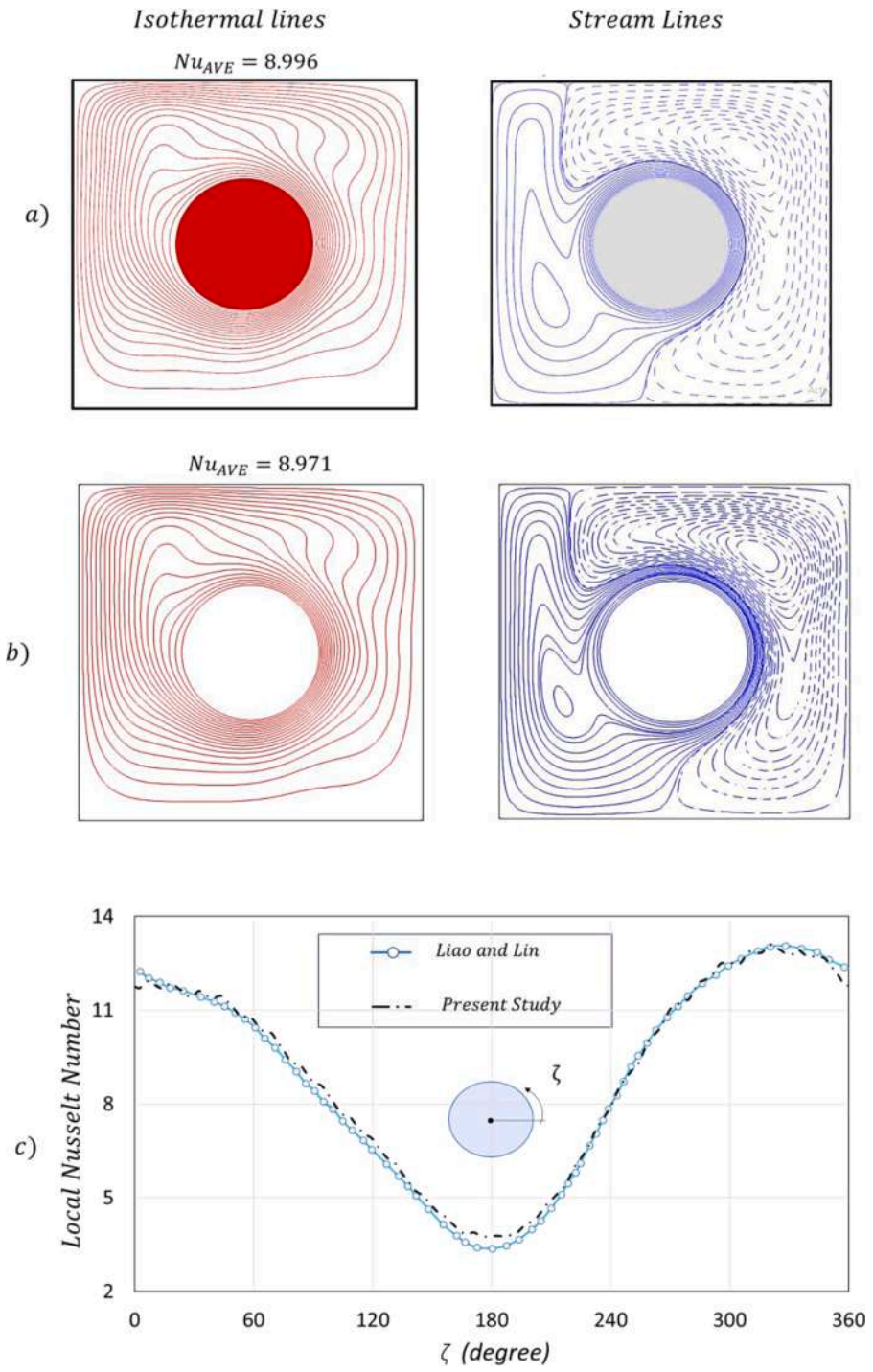

Fig. 5. Streamlines, Nu_{Ave} and isothermal lines of mixed-convection for $Ri = 10$, $Ra = 10^5$, $H/r = 2.5$, *and* $Pr = 0.71$ for (a). Liao and Lin [50], (b). Present work, and (c). Comparison of local Nusselt number on the hot circular wall between the studies.

isothermal lines are separated in most areas. By changing the isothermal lines, the melting zone has also shifted.

Fig. 9 depicts the effect of *Re* numbers. In this case, the isothermal lines and the Cr contours are centered and relatively symmetrical. When the forced convection flow is predominant, $\frac{U}{r\omega} \cong 1$, as Reynolds increases, isothermal lines accumulate near the walls and the heat transfer rate improves. Changes in isothermal lines also cause shifts in the melting zone of nano-capsules. Thus, when melting occurs in the middle of the distance between the cold and hot walls, the melting thickness is higher for Re=50. But at Re=0.5 and the closer of walls, the melting thickness of nano-capsules is higher than Re=50.

Fig. 10 is presented to investigate the values of χ on isothermal lines and Cr contours. By decreasing the values of χ, the maximum values of Cr increase. It is also observed that Cr change causes shifts in the pattern of isothermal lines. It should be noted that θ_f, same as χ, also causes changes in isothermal lines. And the effect of these two parameters is that in the melting zone, isothermal lines are spaced apart and compressed near the wall. At $\theta_f = 0.5$, decreasing χ increases the melting thickness and increases Cr values.

The Nu number diagram for 135 samples is shown in Fig. 11. By decreasing χ, the Nu in all samples enhances or at least remains constant. According to Fig. 10, decreasing χ causes the maximum of Cr to increase

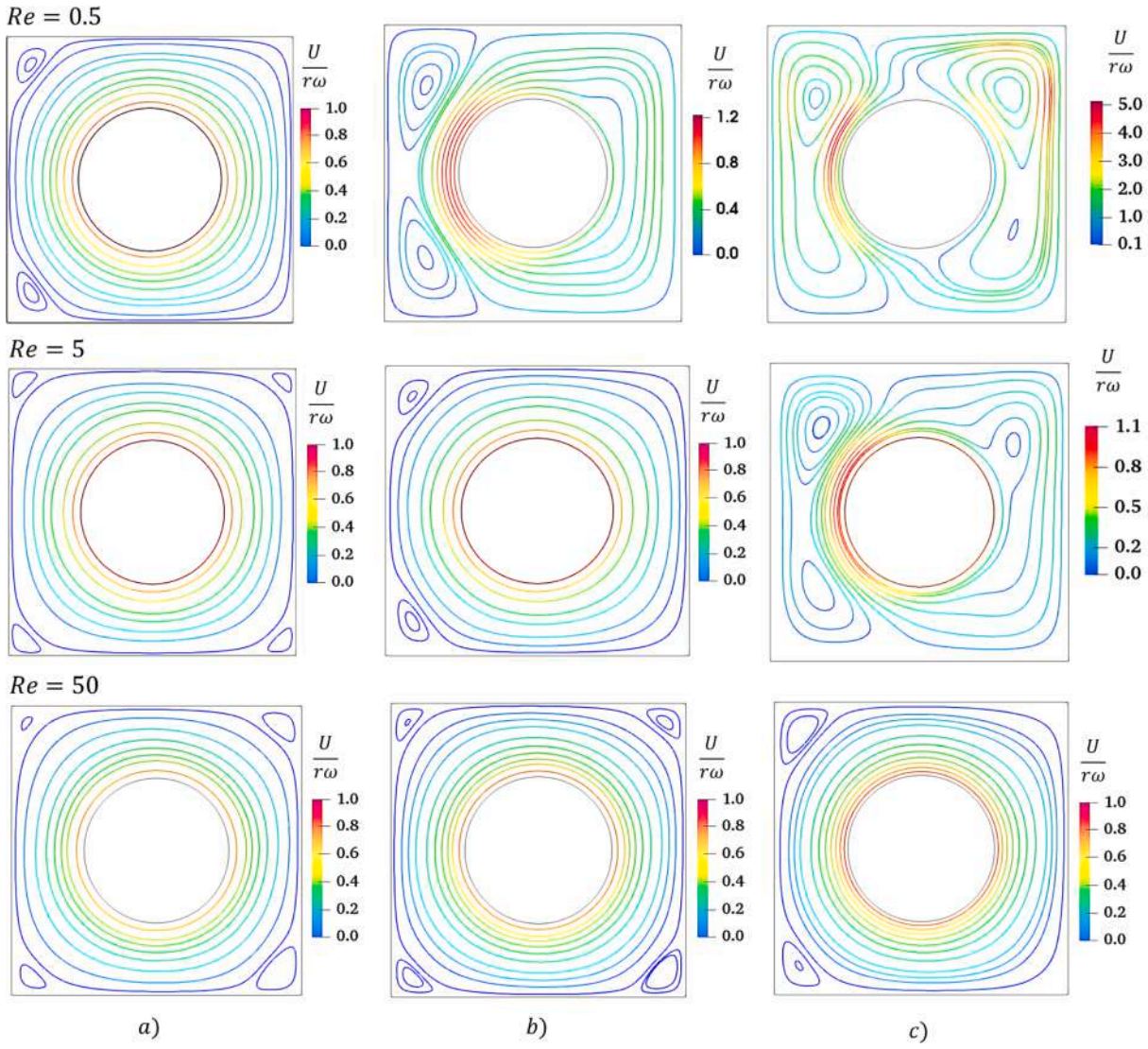

Fig. 6. Streamlines for $\chi = 0.02$, and $\theta_f = 0.5$ and different *Re* numbers at (a). $Gr = 10^2$, (b). $Gr = 10^3$, and (c).$Gr = 10^4$.

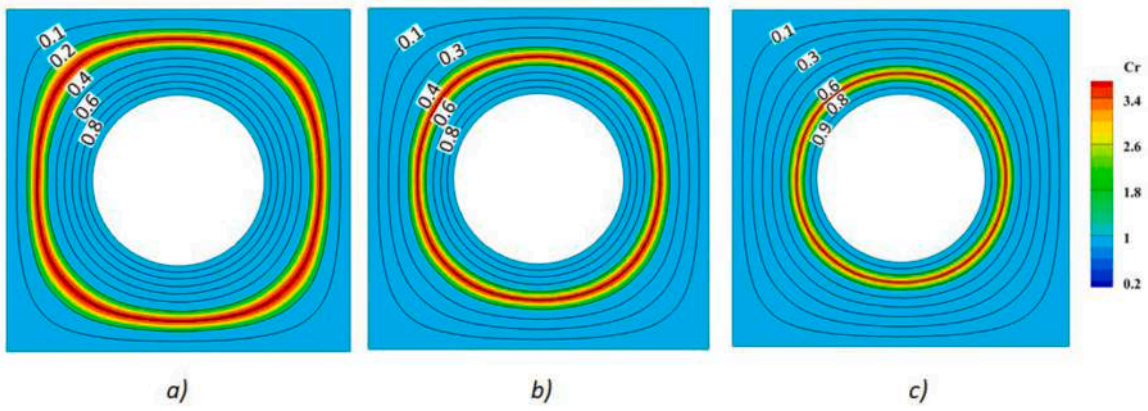

Fig. 7. Non-dimensional isothermal lines (solid lines) and Cr contour for *Re=50, Gr=100,* and $\chi = 0.02$ at (a).$\theta_f = 0.3$, (b).$\theta_f = 0.5$, and (c).$\theta_f = 0.7$.

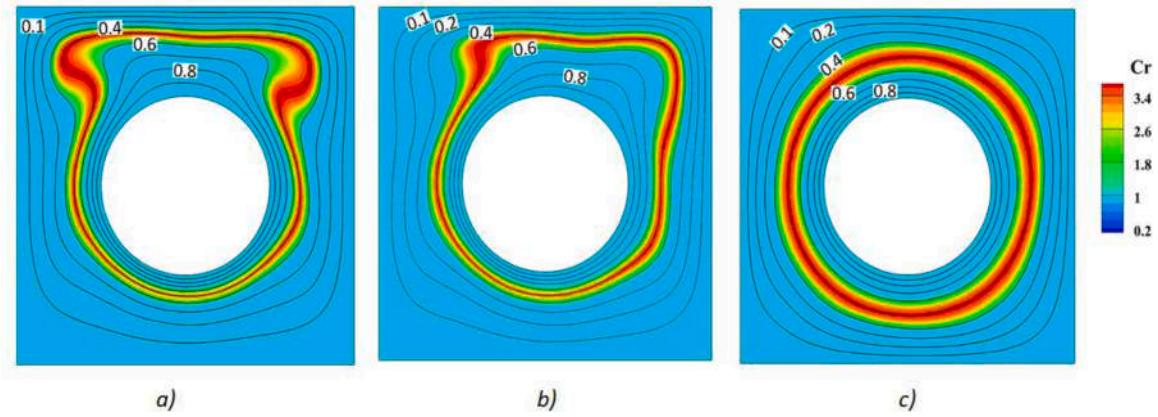

Fig. 8. Non-dimensional isothermal lines (solid lines) and Cr contour for $Gr = 10^4$, $\theta_f = 0.5$, and $\chi = 0.02$ *at* (a).$Re = 0.5$, (b).$Re = 5$, and (c).$Re = 50$.

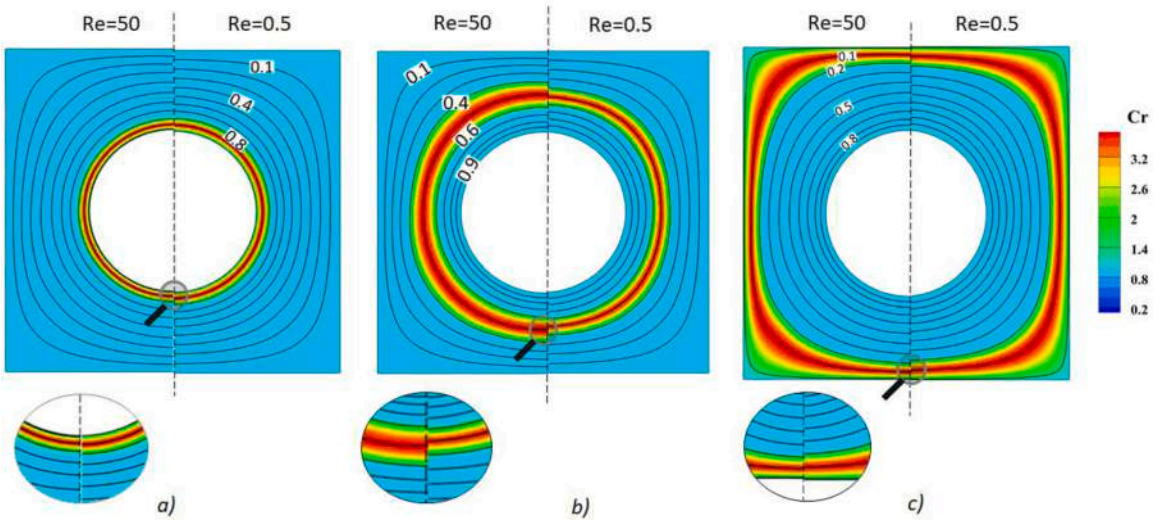

Fig. 9. Comparison of non-dimensional isothermal lines (solid lines) and Cr contour at different *Re* numbers for $Gr = 10^2$, and $\chi = 0.02$ *at* (a).$\theta_f = 0.9$, (b).$\theta_f = 0.5$, and(c).$\theta_f = 0.1$.

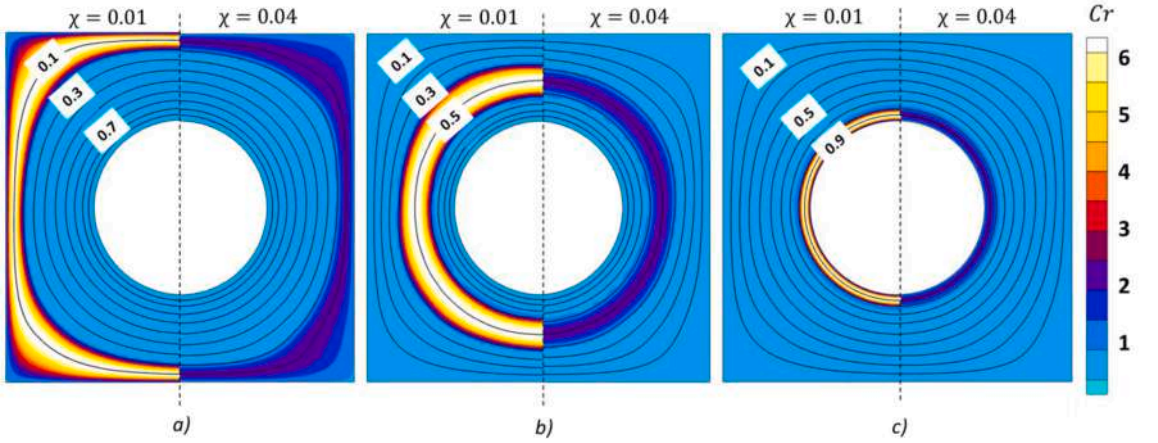

Fig. 10. Comparison of non-dimensional isothermal lines (solid lines) and Cr contour at different χ numbers for $Gr = 10^2$, and $Re = 50$ at (a). $\theta_f = 0.9$, (b). $\theta_f = 0.5$, and (c). $\theta_f = 0.1$.

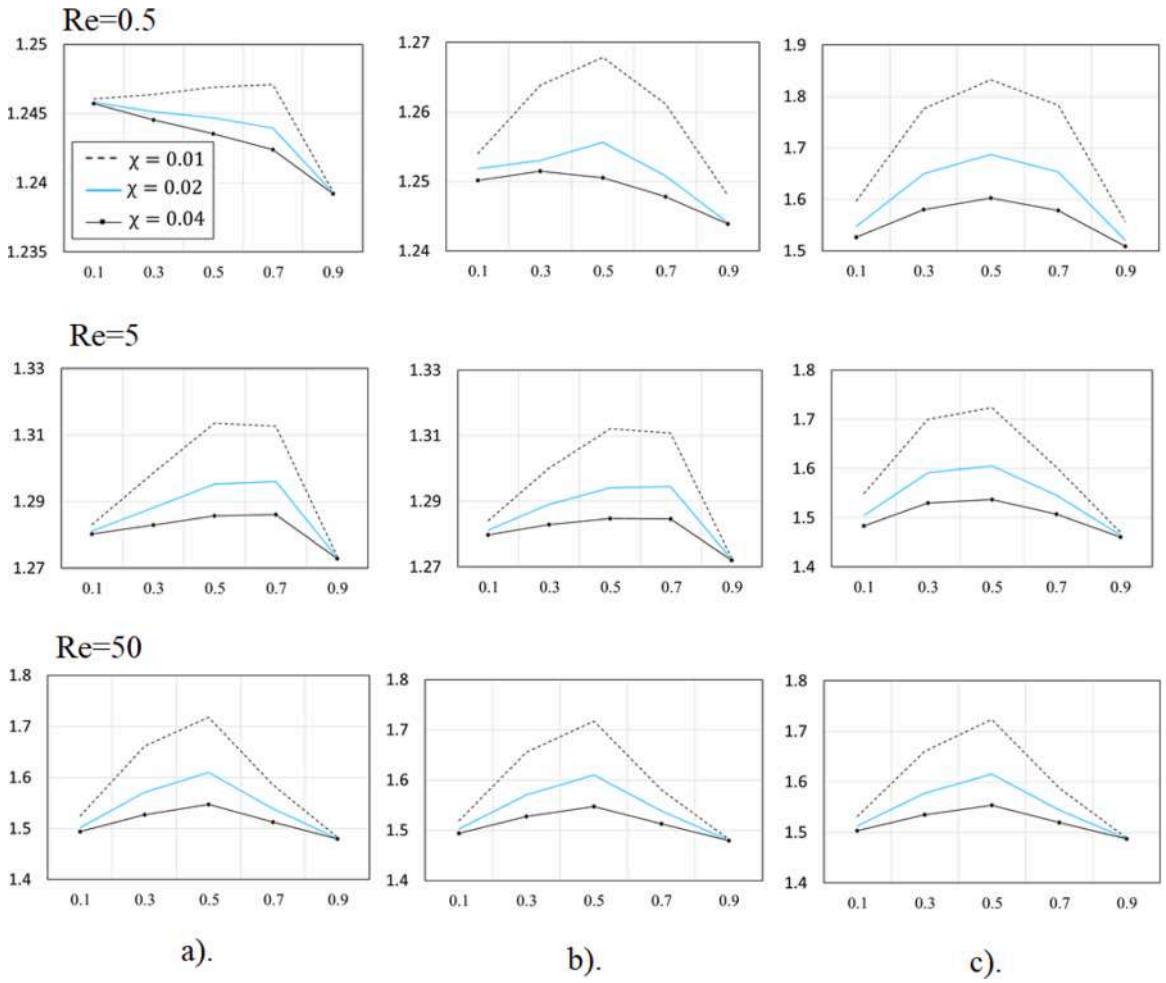

Fig. 11. Average Nusselt number (vertical axis) versus θ_f (horizontal axis) for different *Re* numbers at (a). $Gr = 10^2$, (b). $Gr = 10^3$, *and* (c).$Gr = 10^4$.

and the thickness of the melting layer of NEPCMs to grow. Based on Fig. 11 increasing the melting thickness and maximum value of Cr improve heat transfer rate. In other words, because at a low χ, the maximum value of Cr is higher, it also increases the Prandtl number of the nanofluid, which improves heat transfer and enhances the Nu number.

Also, the density of isothermal lines in the melting zone is affected by χ, and as χ decreases, these lines in the melting zone diverge and accumulate near the walls. where effects similar to Reynolds increase (Fig. 9). In other words, decreasing χ causes the temperature gradient near the walls to increase and more heat to be transferred. As a result, decreasing χ values affects two factors. The first factor raises the maximum Cr and the second factor that increases the melting thickness. In different samples, χ has different effects on Nu number, depending on how each of the two factors is affected. In some cases, two Nu increment factors were affected, such as Nu numbers for $\theta_f = 0.5$ in all *Re* and *Gr* numbers. It was observed that decreasing χ causes a raise in Cr and melting thickness, which enhances Nu. In a series of cases and where θ_f is high or low (not in moderate range), for example, $\theta_f = 0.1,\ 0.9$ in all *Re* and *Gr* numbers χ does not have a significant effect on Nu. In other words, since the reduction of χ causes the isothermal lines to be closer to the walls. As a result, at high or low θ_f, by decreasing χ a lower increasing in melting thickness and Cr has been observed. These two neutralizing factors cause χ do not have much effect on Nu at low or high θ_f.

In the case where conduction is predominant and the isothermal lines are equidistant from each other, increasing θ_f has a relatively linear effect with a negative slope on Nu numbers. The reason is that with increasing θ_f, melting occurs near the inner cylinder, and because the melting is almost circular, this reduces the radius of the melted circle, thus reducing the melting percentage of nano-capsules and causes a decrease in Nu. By increasing *Gr* and *Re* numbers, the convection heat transfer mechanism dominates the conduction and the effect of θ_f changes. In most cases, the highest Nu number observes at $\theta_f = 0.5$ (In some cases, such as $Re = 5$, $Gr = 10^3$, $\chi = 0.02$, it occurs at $\theta_f = 0.7$). The diagram of Nu versus θ_f is almost parabolic. The effect of θ_f is more noticeable at low χ numbers. As *Gr* and *Re* numbers increase, Nu numbers enhance. However, in $Gr = 10^4$ it decreases Nu with increasing *Re*. This is due to the reduction in velocity and resistance of natural convection flow to forced convection by increasing *Re* number (See Figs. 6 and 9). It is noteworthy at the end of the work that the results of this work can be generalized to adsorption studies, artificial recharge structures and etc. [53–55].

4. Conclusion

In this study, we investigated the effects of adding NEPCMs on mixed-convection heat transfer. The geometry consisted of a square chamber with an outer wall of constant and low temperature. Also, a hot internal cylinder was rotating. We evaluate the performance of NEPCMs by considering the different scenarios of the effects of natural and forced convection flow. In this study, based on the evaluations performed in 135 samples, the following results were adopted. Increasing χ has a negative effect on Nusselt number. The effects of χ are clearly affected by

the values of θ_f. In moderate θ_f and close to 0.5, χ reduction greatly improves Nusselt number. However, at high or low $\theta_f s$, the effects of χ fade. The relation θ_f to Nusselt numbers is almost similar to a negative concavity parabolic diagram. The optimal state of θ_f is in medium values or particularly numbers close to 0.5. In low *Gr* and *Re* number when conduction is effective and if χ is high, the optimal state of θ_f occurs in values close to 0.1. Increasing *Re* and *Gr* numbers improved heat transfer rate. However, in high *Gr* number, increasing the rotation velocity of the inner cylinder, consequently increasing *Re* number, reduced Nusselt.

CRediT authorship contribution statement

Arsalan Nasiri Sadr: Methodology, Software, Validation, Writing – review & editing, Investigation. **Masih Shekaramiz:** Methodology, Writing – original draft, Software, Validation, Writing – review & editing, Investigation. **Meysam Zarinfar:** Methodology, Writing – original draft, Software, Validation, Writing – review & editing, Investigation. **Amin Esmaily:** Methodology, Writing – original draft, Software, Validation, Writing – review & editing, Investigation. **Hamidreza Khoshtarash:** Methodology, Writing – original draft, Software, Validation, Writing – review & editing, Investigation. **Davood Toghraie:** Methodology, Software, Writing – original draft, Validation, Writing – review & editing, Investigation.

Declaration of Competing Interest

The authors declare that they have no known competing financial interests or personal relationships that could have appeared to influence the work reported in this paper.

References

[1] R. Kalbasi, Introducing a novel heat sink comprising PCM and air-Adapted to electronic device thermal management, Int. J. Heat Mass Tran. 169 (2021) 120914.
[2] M.R. Salimpour, R. Kalbasi, G. Lorenzini, Constructal multi-scale structure of PCM-based heat sinks, Contin. Mech. Thermodyn. 29 (2) (2017) 477–491.
[3] A.S. Rad, A. Shadravan, A.A. Soleymani, N. Motaghedi, Lewis acid-base surface interaction of some boron compounds with N-doped graphene; first principles study, Curr. Appl. Phys. 15 (10) (2015) 1271–1277.
[4] C.J. Ho, Y.W. Guo, T.F. Yang, S. Rashidi, W.M. Yan, Numerical study on forced convection of water-based suspensions of nanoencapsulated PCM particles/Al_2O3 nanoparticles in a mini-channel heat sink, Int. J. Heat Mass Transf. 157 (2020), 119965.
[5] A. Shokrolahzade Tehrani, A. Shadravan, M. Kashefi Asl, Investigation of kinetics and isotherms of boron adsorption of water samples by natural clinoptilolite and clinoptilolite modified with sulfuric acid, Nashr. Shimi Mohan. Shimi Iran 35 (4) (2017) 21–32.
[6] T. Jiang, Z. Liu, G. Wang, Z. Chen, Comparative study of thermally stratified tank using different heat transfer materials for concentrated solar power plant, Energy Rep. 7 (2021) 3678–3687.
[7] E. Alehosseini, S.M. Jafari, Micro/nano-encapsulated phase change materials (PCMs) as emerging materials for the food industry, Trends Food Sci. Technol. 91 (2019) 116–128.
[8] H.R. Seyf, Z. Zhou, H.B. Ma, Y. Zhang, Three dimensional numerical study of heat-transfer enhancement by nano-encapsulated phase change material slurry in microtube heat sinks with tangential impingement, Int. J. Heat Mass Transf. 56 (1–2) (2013) 561–573.
[9] R. Sabbah, M.M. Farid, S. Al-Hallaj, Micro-channel heat sink with slurry of water with micro-encapsulated phase change material: 3D-numerical study, Appl. Therm Eng. 29 (2–3) (2009) 445–454.
[10] H. Reza Seyf, M.R. Wilson, Y. Zhang, H.B. Ma, Flow and heat transfer of nanoencapsulated phase change material slurry past a unconfined square cylinder, J. Heat Transf. 136 (5) (2014), 051902.
[11] S.M.H. Zadeh, S.A.M. Mehryan, M.S. Islam, M. Ghalambaz, Irreversibility analysis of thermally driven flow of a water-based suspension with dispersed nano-sized capsules of phase change material, Int. J. Heat Mass Transf. 155 (2020), 119796.
[12] K. Kant, A. Shukla, A. Sharma, P.H. Biwole, Heat transfer study of phase change materials with graphene nano particle for thermal energy storage, Sol. Energy 146 (2017) 453–463.
[13] D. Huu-Quan, M. Sheremet, M.S. Kamel, M. Izadi, Investigation of thermal-hydro dynamical behavior on nano-encapsulated PCM suspension: effect of fin position, fractioning and aspect ratio, Chem. Eng. Process.-Process Intensif. 157 (2020), 108122.
[14] M. Ghalambaz, S.A.M. Mehryan, I. Zahmatkesh, A. Chamkha, Free convection heat transfer analysis of a suspension of nano–encapsulated phase change materials (NEPCMs) in an inclined porous cavity, Int. J. Therm. Sci. 157 (2020), 106503.
[15] S.E. Ahmed, H.M. Elshehabey, Buoyancy-driven flow of nanofluids in an inclined enclosure containing an adiabatic obstacle with heat generation/absorption: effects of periodic thermal conditions, Int. J. Heat Mass Transf. 124 (2018) 58–73.
[16] M. Ghalambaz, S.A.M. Mehryan, M. Mozaffari, A. Hajjar, M. El Kadri, N. Rachedi, M. Sheremet, O. Younis, S. Nadeem, Entropy generation and natural convection flow of a suspension containing nano-encapsulated phase change particles in a semi-annular cavity, J. Energy Storage 32 (2020), 101834.
[17] M. Ghalambaz, T. Groşan, I. Pop, Mixed convection boundary layer flow and heat transfer over a vertical plate embedded in a porous medium filled with a suspension of nano-encapsulated phase change materials, J. Mol. Liq. 293 (2019), 111432.
[18] Z. Raizah, A.M. Aly, Double-diffusive convection of a rotating circular cylinder in a porous cavity suspended by nano-encapsulated phase change materials, Case Stud. Therm. Eng. 24 (2021), 100864.
[19] S.E. Ahmed, Z.A. Raizah, Analysis of the entropy due to radiative flow of nano–encapsulated phase change materials within inclined porous prismatic enclosures: finite element simulation, J. Energy Storage 40 (2021), 102719.
[20] C. Fu, A. Rahmani, W. Suksatan, S.M. Alizadeh, M. Zarringhalam, S. Chupradit, et al., Comprehensive investigations of mixed convection of Fe–ethylene-glycol nanofluid inside an enclosure with different obstacles using lattice Boltzmann method, Scientific Reports 11 (1) (2021) 1–16.
[21] B. Ruhani, D. Toghraie, M. Hekmatifar, M. Hadian, Statistical investigation for developing a new model for rheological behavior of ZnO–Ag (50%–50%)/Water hybrid Newtonian nanofluid using experimental data, Physica A 525 (2019) 741–751.
[22] T. Tjahjono, M. Elveny, S. Chupradit, D. Bokov, H.T. Hoi, M. Pandey, Role of cryogenic cycling rejuvenation on flow behavior of ZrCuAlNiAg metallic glass at relaxation temperature, Trans. Indian Inst. Met. (2021) 1–7.
[23] A. Lincy, P. Jegathambal, M. Mkandawire, S. MacQuarrie, Nano bioremediation of textile dye effluent using magnetite nanoparticles encapsulated alginate beads, J. Environ. Treat. Tech. 8 (3) (2020) 936–946.
[24] Al-Shawi Sarmad Ghazi, N. Andreevna Alekhina, S. Aravindhan, L. Thangavelu, A. Elena, N. Viktorovna Kartamysheva, et al., Synthesis of NiO Nanoparticles and Sulfur, and Nitrogen co Doped-Graphene Quantum Dots/NiO Nanocomposites for Antibacterial Application, J. Nanostruct. 11 (1) (2021) 181–188.
[25] S. Hutapea, S. Ghazi Al-Shawi, T.C. Chen, X. You, D. Bokov, W.K. Abdelbasset, et al., Study on food preservation materials based on nano-particle reagents, Food Sci. Technol. (2021), https://doi.org/10.1590/fst.39721.
[26] Y. Zhu, X. Zheng, Y. Lu, X. Yang, A. Kheradmand, Y. Jiang, Efficient upconverting carbon nitride nanotubes for near-infrared-driven photocatalytic hydrogen production, Nanoscale 11 (2019) 20274.
[27] A. Kheradmand, Y. Zhu, W. Zhang, A. Marianov, Y. Jiang, Cobalt oxide on mesoporous carbon nitride for improved photocatalytic hydrogen production under visible light irradiation, Int. J. Hydrog. Energy 44 (2019) 17930.
[28] S.A. Haddadi, A.S.A. Ramazani, A. Kheradmand, M. Amini, M. Ramezanzadeh, SiO_2-covered graphene oxide nanohybrids for in situ preparation of UHMWPE/GO (SiO_2) nanocomposites with superior mechanical and tribological properties, J. Appl. Polym. Sci. 136 (2019) 47796.
[29] M. Amini, A.S.A. Ramazani, S.A. Haddadi, A. Kheradmand, Mechanical, rheological and oxygen barrier properties of ethylene vinyl acetate/diamond nanocomposites for packaging applications, Diam Relat. Mater. 99 (2019) 107523.
[30] A. Kheradmand, A. Wainwright, L. Wang, Y. Jiang, Anchoring iron oxides on carbon nitride nanotubes for improved photocatalytic hydrogen production, Energy Fuels 35 (2021) 868.
[31] N. Ngafwan, H. Rasyid, E.S. Abood, W.K. Abdelbasset, S.G. Al-Shawi, D. Bokov, A. T. Jalil, Study on novel fluorescent carbon nanomaterials in food analysis, Food Sci. Technol (2021), https://doi.org/10.1590/fst.37821.
[32] A. Shahsavar, A. Godini, P.T. Sardari, D. Toghraie, H. Salehipour, Impact of variable fluid properties on forced convection of Fe_3O_4/CNT/water hybrid nanofluid in a double-pipe mini-channel heat exchanger, J. Therm. Anal. Calorim. 137 (3) (2019) 1031–1043.
[33] M. Ghalambaz, A.J. Chamkha, D. Wen, Natural convective flow and heat transfer of nano-encapsulated phase change materials (NEPCMs) in a cavity, Int. J. Heat Mass Transf. 138 (2019) 738–749.
[34] S.Y. Motlagh, E. Golab, A.N. Sadr, Two-phase modeling of the free convection of nanofluid inside the inclined porous semi-annulus enclosure, Int. J. Mech. Sci. 164 (2019), 105183.
[35] M.H. Ahmadi, B. Mohseni-Gharyehsafa, M. Ghazvini, et al., Comparing various machine learning approaches in modeling the dynamic viscosity of CuO/water nanofluid, J. Therm. Anal. Calorim. 139 (2020) 2585–2599, https://doi.org/10.1007/s10973-019-08762-z.
[36] S.O. Giwa, M. Sharifpur, M. Goodarzi, et al., Influence of base fluid, temperature, and concentration on the thermophysical properties of hybrid nanofluids of alumina–ferrofluid: experimental data, modeling through enhanced ANN, ANFIS, and curve fitting, J. Therm. Anal. Calorim. 143 (2021) 4149–4167, https://doi.org/10.1007/s10973-020-09372-w.
[37] A novel sensitivity analysis model of EANN for F-MWCNTs–Fe3O4/EG nanofluid thermal conductivity: outputs predicted analytically instead of numerically to more accuracy and less costs.
[38] Configuration and optimization of a minichannel using water-alumina nanofluid by non-dominated sorting genetic algorithm and response surface method.
[39] A. Piquet, B. Zebiri, A. Hadjadj, M. Safdari Shadloo, A parallel high-order compressible flows solver with domain decomposition method in the generalized curvilinear coordinates system, Int. J. Numer. Methods Heat Fluid Flow 30 (1) (2020) 2–38, https://doi.org/10.1108/HFF-01-2019-0048.

[40] H. Eshgarf, R. Kalbasi, A. Maleki, et al., A review on the properties, preparation, models and stability of hybrid nanofluids to optimize energy consumption, J. Therm. Anal. Calorim. 144 (2021) 1959–1983, https://doi.org/10.1007/s10973-020-09998-w.
[41] M. Hopp-Hirschler, M. SafdariShadloo, U. Nieken, A smoothed particle hydrodynamics approach for thermo-capillary flows, Comput. Fluids 176 (2018) 1–19.
[42] A. Piquet, B. Zebiri, A. Hadjadj, M. Safdari Shadloo, A parallel high-order compressible flows solver with domain decomposition method in the generalized curvilinear coordinates system, Int. J. Numer. Methods Heat Fluid Flow 30 (1) (2020) 2–38, https://doi.org/10.1108/HFF-01-2019-0048.
[43] H. Li, X. Liu, G. Fang, Preparation and characteristics of n-nonadecane/cement composites as thermal energy storage materials in buildings, Energy Build. 42 (10) (2010) 1661–1665.
[44] P.F. De Castro, D.G. Shchukin, New polyurethane/docosane microcapsules as phase-change materials for thermal energy storage, Chemistry 21 (31) (2015) 11174–11179.
[45] E.M. Shchukina, M. Graham, Z. Zheng, D.G. Shchukin, Nanoencapsulation of phase change materials for advanced thermal energy storage systems, Chem. Soc. Rev. 47 (11) (2018) 4156–4175.
[46] S. Barlak, O.N. Sara, A. Karaipekli, S. Yapıcı, Thermal conductivity and viscosity of nanofluids having nanoencapsulated phase change material, Nanoscale Microscale Thermophys. Eng. 20 (2) (2016) 85–96.
[47] S. Barlak, A. Karaipekli, O.N. Sara, S. Yapici, Preparation and characterization of nanoencapsulated n-nonadecane for convective heat transfer. Progress in Clean Energy, Springer, Cham, 2015, pp. 403–411. Volume 1.
[48] S.E. Ahmed, M.A. Mansour, A.K. Hussein, B. Mallikarjuna, M.A. Almeshaal, L. Kolsi, MHD mixed convection in an inclined cavity containing adiabatic obstacle and filled with Cu–water nanofluid in the presence of the heat generation and partial slip, J. Therm. Anal. Calorim. 138 (2) (2019) 1443–1460.
[49] S.E. Ahmed, M. Alhazmi, Impacts of the rotation and various thermal conditions of cylinders within lid-driven enclosures filled with glass balls in the presence of radiation: FEM simulation, Int. Commun. Heat Mass Transf. 128 (2021), 105603.
[50] C.C. Liao, C.A. Lin, Mixed convection of a heated rotating cylinder in a square enclosure, Int. J. Heat Mass Transf. 72 (2014) 9–22.
[51] G.A. Sheikhzadeh, M. Dastmalchi, H. Khorasanizadeh, Effects of nanoparticles transport mechanisms on Al_2O_3–water nanofluid natural convection in a square enclosure, Int. J. Therm. Sci. 66 (2013) 51–62.
[52] C.J. Ho, W.K. Liu, Y.S. Chang, C.C. Lin, Natural convection heat transfer of alumina-water nanofluid in vertical square enclosures: an experimental study, Int. J. Therm. Sci. 49 (8) (2010) 1345–1353.
[53] S. Rajoriya, A. Haquiqi, B. Chauhan, G. Tyagi, A.S. Pundir, A.K. Jain, Adsorption Studies on the removal of hexavalent chromium (Cr (VI)) from aqueous solution using black gram husk, J. Environ. Treat. Tech. 8 (3) (2020) 1144–1150.
[54] Z. Tao, Z. Cui, J. Yu, M. Khayatnezhad, Finite difference modelings of groundwater flow for constructing artificial recharge structures, IJST-T CIV ENG. (2021) 1–12.
[55] X. Yi-Peng, P. Ouyang, S.M. Xing, L.Y. Qi, H. Jafari, Optimal structure design of a PV/FC HRES using amended Water Strider Algorithm, Energy Reports 7 (2021) 2057–2067.